A mathematical model relating cortical oxygenated and deoxygenated hemoglobin flows and volumes to neural activity

2015 J. Neural Eng. 12 046013

(http://iopscience.iop.org/1741-2552/12/4/046013)

IOP Publishing Journal of Neural Engineering
J. Neural Eng. 12 (2015) 046013 (17pp) doi:10.1088/1741-2560/12/4/046013

A mathematical model relating cortical oxygenated and deoxygenated hemoglobin flows and volumes to neural activity

Nathan R Cornelius[1], Nozomi Nishimura[1], Minah Suh[2], Theodore H Schwartz[3] and Peter C Doerschuk[4,5]

[1] Department of Biomedical Engineering, Weill Hall, Cornell University, Ithaca, NY 14853, USA
[2] Center for Neuroscience Imaging Research (CNIR), Institute for Basic Science (IBS), Department of Biomedical Engineering, Department of Biological Science, Sungkyunkwan University, Suwon 440-746, Korea
[3] Department of Neurological Surgery, Weill Cornell Medical College, New York Presbyterian Hospital, 525 East 68th St., Box #99, New York, NY 10065, USA
[4] Department of Biomedical Engineering, School of Electrical and Computer Engineering, Weill Hall, Cornell University, Ithaca, NY 14853, USA

E-mail: nrc23@cornell.edu, nn62@cornell.edu, minahsuh@skku.edu, schwarh@med.cornell.edu and pd83@cornell.edu

Received 17 October 2014, revised 27 April 2015
Accepted for publication 5 May 2015
Published 3 June 2015

Abstract

Objective. To describe a toolkit of components for mathematical models of the relationship between cortical neural activity and space-resolved and time-resolved flows and volumes of oxygenated and deoxygenated hemoglobin motivated by optical intrinsic signal imaging (OISI). *Approach.* Both blood flow and blood volume and both oxygenated and deoxygenated hemoglobin and their interconversion are accounted for. Flow and volume are described by including analogies to both resistive and capacitive electrical circuit elements. Oxygenated and deoxygenated hemoglobin and their interconversion are described by generalization of Kirchhoff's laws based on well-mixed compartments. *Main results.* Mathematical models built from this toolkit are able to reproduce experimental single-stimulus OISI results that are described in papers from other research groups and are able to describe the response to multiple-stimuli experiments as a sublinear superposition of responses to the individual stimuli. *Significance.* The same assembly of tools from the toolkit but with different parameter values is able to describe effects that are considered distinctive, such as the presence or absence of an initial decrease in oxygenated hemoglobin concentration, indicating that the differences might be due to unique parameter values in a subject rather than different fundamental mechanisms.

Keywords: neurovascular model, optical intrinsic signal imaging, cerebral blood flow control, cerebral blood volume control

(Some figures may appear in colour only in the online journal)

1. Introduction

Optical intrinsic signal imaging (OISI) is essentially microscopic video reflectance spectroscopy imaging of exposed brain cortex and has been done on patients being prepared for neurosurgery for the treatment of intractable epilepsy as well as more extensively on experimental animals during the study of the neurovascular coupling of cerebral blood volume, hemoglobin oxygenation, and neuronal activity.

The ultimate goal of this work is to contribute to the planning of neurosurgical procedures. A patient with epilepsy that is intractable to drug therapy is sometimes treated by

[5] Author to whom any correspondence should be addressed.

surgical removal of the initiating focus of the seizures. After preoperative diagnostic studies, such a patient can have additional diagnostic tests done after the region of cortex has been exposed by a craniotomy but before removal of any neural tissue, including OISI [1–6], in order to improve the surgical plan. Moreover, OISI may used to examine and quantify the effect of electrical neurostimulation to increase blood flow in the brain. Both of these applications involve the behavior of the mathematical model of the neurovascular system over extended periods of time. Because of the duration, this paper describes and demonstrates new lumped-parameter circuit models for the flows and volumes of oxygenated and deoxygenated hemoglobin coupled to a neurovascular control system based on feedback and therefore representing the so-called metabolic hypothesis [7] for neurovascular control. The ultimate goal is not achieved in this paper because of challenges in extracting accurate vessel topologies from the OISI imagery. Therefore the tools developed in this paper are demonstrated in simpler situations (sections 3 and 4). Because the model is motivated by human neurosurgery applications, the goal is an approach that is sufficiently simple such that the parameters in the model can be determined for individual subjects, e.g., for intra-operative clinical video [6] from a patient, rather than for populations of subjects.

In order to achieve the simplicity goals, the model is based on a combination of physical laws, including Kirchhoff's, Laplace's, Poiseuille's, and Beer–Lambert laws, and phenomenological relationships. Because the neurovascular interaction is not completely understood, a goal is to provide a set of tools that are sufficiently flexible such that different hypotheses can be explored computationally, analogous to the flexibility of the models of [8].

Models of the neurovascular system typically involve many components and different components are modeled by different investigators with different levels of physical fidelity. For instance, the network topology of [9] is based on x-ray synchrotron images of 2.8 mm^3 volumes of rat cortex and networks of similar fidelity are probably also available via two-photon laser scanning microscopy (TPLSM) [10, 11]. The networks used in the numerical examples of this paper are much more idealized, but the circuit ideas could be used in much more complicated and realistic networks. Some investigations focused on flows use purely resistive models [9] while other models based on balloons [12] and windkessel [13] ideas combine resistors and capacitors. In addition, some models describe input–output phenomenological behavior [8, 14–16] while others focus on individual vessels [9, 17]. The model described in this paper is focused on individual vessel segments and describes the segments with circuits including both resistance and capacitance. However, the 3D geometry of the vessel segment is only approximated, i.e., what fraction of the vessel appears in what pixel of the image data. It would be challenging to infer more information from the image data and probably not necessary to have more information in order to achieve the goal of predicting the aggregated signal in a pixel of the image data. Some investigators include extensive biochemistry in their models [18]. While the biochemistry in the model described in this paper is limited to the conversion of HbO_2 to HbR, additional molecules that are transported by the entering blood and metabolized dependent on brain activity could be included (section 2.2.3).

The remainder of the paper is organized in the following fashion. The model is described in section 2. Comparisons with two sets of experimental data are described in section 3 and example calculations demonstrating the spatial features of the model are also described in section 3. Grubb's law [19] is a macroscopic time-averaged relationship between cerebral blood volume and cerebral blood flow originally described in 1974 based on radioactive tracer analysis. The model of this paper makes it possible to compute many quantities related to cerebral blood volume and cerebral blood flow. As an example of such a calculation, in section 4 we derive a relationship between cerebral blood volume and flow analogous to Grubb's law. Finally, the paper concludes with a discussion (section 5).

2. Model

The OISI signal is dominated by the oxygenation state of hemoglobin. Therefore, the information that is available from these measurements is space-resolved and time-resolved blood flow, blood volume, and hemoglobin oxygen-saturation values. The level of detail described in the model is specified by the detail of the experiments. The experiment allows pixel sizes on the order of 10^1 μm and temporal sampling intervals on the order of 10^{-1} s. Such pixel sizes are on the same order of magnitude as a typical capillary length and therefore a capillary may contribute to multiple pixels thereby acting to deliver hemoglobin with intermediate oxygenation level to the more distal pixel(s). Therefore the circuit elements and laws are designed to provide corresponding levels of detail. The temporal sampling interval is intermediate between the intervals of MRI (typically 10^0 s) and ECG or MEG (typically 10^{-3} s). Because the saturation state of hemoglobin is an important feature of the experiment, it is also an important feature of the modeling tools. But it would be straightforward to take the ideas of the modeling tools and apply them to other molecules. Finally, the experiment reflects the nonlinear nature of the neurovascular coupling and therefore the resulting model is also nonlinear. Because of the nonlinearity, the model describes total signals and not perturbations in signals superimposed on an unmodeled baseline signal.

The model has four components as is shown in figure 1. The first two components are a vascular circuit that describes cerebral blood flows and volumes and a control system modifies parameters in the circuit. These two components are the primary focus of the paper. The second two components are a description of the neural electrical signals that drive the first two components and a description of the optical system that provides measurements of the vascular circuit component.

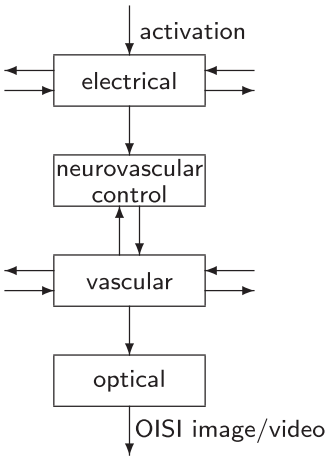

Figure 1. The four components of the model at one pixel and their interactions shown as arrows which indicate the direction of the interaction. The horizontal arrows indicate connections to adjacent pixels.

2.1. Model: vascular component

A circuit is described in terms of elements, interconnection laws, and topology. The novelty in the vascular circuit is concentrated in the elements, in which resistance to flow and storage of volume are controlled by a single parameter, and the interconnection laws, where flows and volumes of oxygenated and deoxygenated hemoglobin are separately described (including the conversion of oxygenated hemoglobin to deoxygenated hemoglobin) since the pixel size is on the same order of magnitude as the length of a capillary leading to a pixel receiving hemoglobin with varying oxygenation levels. In some cases, very simple topologies are used, e.g., in describing the macroscopic Grubb's law [19]. If detailed topology is available for a situation of interest, the components and connections between components described in this paper could be easily inserted.

2.1.1. Circuit elements. There are detailed models of the vascular wall. For instance, reference [8] describes a visco-elastic model artery, capillary, and venous components. Reference [20] describes a nonlinear elastic model for larger arteries focused on describing the changes that occur in arterial wall hypertrophy associated with systemic hypertension. Reference [21] describes a visco-elastic model of primarily the venous compartment where one of the parameters in the pressure-volume relationship of the vessel is given its own phenomenological temporal differential equation. All of these models are focused on temporal variation of a vascular system without spatial extent so, in the context of OISI video data, they would perhaps be models for each pixel or each vessel segment within a pixel. However, unless the parameters do not have to be altered from nominal values even for ill patients, there are too many parameters to be estimated for each vessel segment in each pixel from the type of OISI data that motivated this work [6]. Therefore we use much simpler, albeit less accurate, models as described in the remainder of this section.

Sources and two types of circuit elements are used to model the vascular system. The simpler type has a fixed volume and resistance to flow (figure 2(a)). The more complicated type has a vascular wall that is described as a linear isotropic elastic material with a Young's modulus which is denoted by E (figure 2(b)). When pressure in the tube increases the tube expands in diameter so that the volume increases and the resistance to flow decreases. Alternatively, when E increases ('stiffer') the diameter decreases and the resistance to flow increases and when E decreases ('floppier') the diameter increases and the resistance to flow decreases. The vascular system is thought of as being controlled by controlling the value of E. In a rough way, this corresponds to controlling the tone of the smooth muscle in the wall of small vessels. In the electrical circuit analogy, fluid flow is electrical current and fluid pressure is electrical voltage.

Tubes with variable Young's modulus. The tube with variable modulus (figure 2(b)) is simultaneously described from two different points of view. In the first point of view, the tube is in equilibrium with a constant pressure throughout and the radius of the elastic wall is determined by the pressure and Young's modulus (denoted by E). Let the Young's modulus be described as $E(t) = E_0 + \delta_E(t)$, where E_0 is the nominal Young's modulus and $\delta_E(t)$ is the perturbation in the Young's modulus due to control. Let ζ be the thickness of the wall. Let a_0 be the nominal and a the actual radius of the tube. Let P be the pressure in the tube. Then, the cylindrical form of Laplace's law [22, p 71] is

$$\frac{aP}{\zeta} = \left(E_0 + \delta_E\right)\frac{a - a_0}{a_0} \tag{1}$$

(the units are P: (Pressure) = (Force/Area^2); E_0 and δ_E: (Force/Area^2); a, a_0, and ζ: (Length)). Solving this equation for a gives a as a function of P and δ_E (as well as the nominal values E_0 and a_0 which are suppressed in the notation), specifically,

$$a\left(P, \delta_E\right) = \frac{E_0 + \delta_E}{\frac{E_0 + \delta_E}{a_0} - \frac{P}{\zeta}}. \tag{2}$$

Let l denote the length of the tube and Q denote the volume of the tube. Then standard geometry (the volume of a cylinder) implies that Q as a function of P and δ_E is

$$Q\left(P, \delta_E\right) = \pi\left[a\left(P, \delta_E\right)\right]^2 l = \pi\left[\frac{E_0 + \delta_E}{\frac{E_0 + \delta_E}{a_0} - \frac{P}{\zeta}}\right]^2 l. \tag{3}$$

$Q(P, \delta_E)$ is the tube's contribution to the blood volume of the cortex imaged in this particular pixel. In the analogy to an electric circuit, changes in $Q(P, \delta_E)$ with time are the charging and discharging of a capacitor with time.

In the second point of view, the tube is in the steady state with a difference of pressure between its ends and a fixed

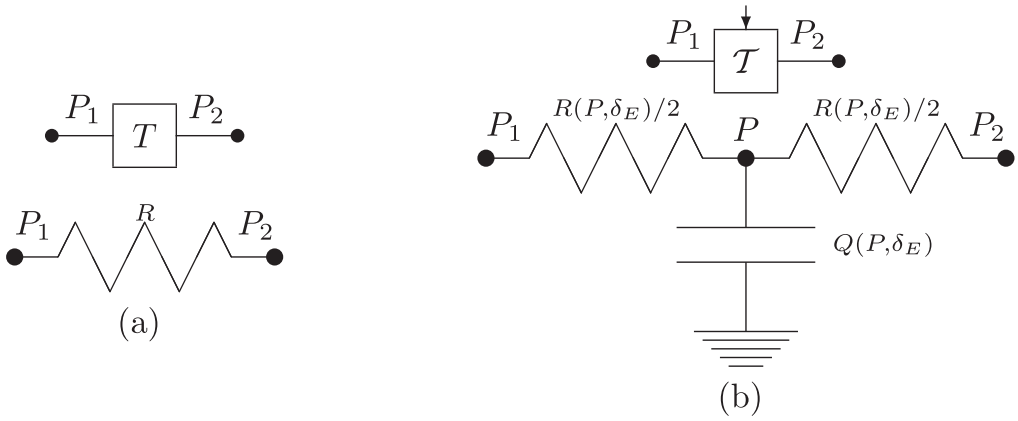

Figure 2. Circuits within vascular tubes. Panel (a): a purely resistive elementary component with fixed modulus (T) in block form and as an electrical circuit. Panel (b): a elementary component with both resistive and capacitive characteristics and a variable modulus ($\mathcal{T}$) in block form and as an electrical circuit. The arrow on the $\mathcal{T}$ block indicates the control signal for the variable modulus.

radius of the elastic wall and the fluid undergoes laminar flow through the tube. Poiseuille's formula [23] states that the pressure drop from one end of the tube to the other end is proportional to the volume flow through the tube. Arbitrarily label the ends of the tube by 1 and 2. Let P_1 and P_2 be the pressures at end 1 and end 2, respectively, of the tube and let I be the volume flow into end 1. (If $I < 0$ then the flow is, in fact, out of end 1.) Let η be the dynamic viscosity of the fluid. Then Poiseuille's formula [22, p 94] is

$$P_1 - P_2 = \frac{8\eta l I}{\pi\left[a\left(P,\,\delta_E\right)\right]^4}. \tag{4}$$

Since the difference of pressures $(P_1 - P_2)$ is linearly related to the flow (I), it is natural to define a resistance which is denoted by $R(P,\,\delta_E)$ and defined by

$$R\left(P,\,\delta_E\right) = \frac{8\eta l}{\pi\left[a\left(P,\,\delta_E\right)\right]^4} = \frac{8\eta l}{\pi}\left[\frac{\frac{E_0+\delta_E}{a_0} - \frac{P}{\zeta}}{E_0+\delta_E}\right]^4. \tag{5}$$

In the eventual electric circuit, $R(P,\,\delta_E)$ is a resistor. Note that the dependence of viscosity η on radius a (e.g., [24, 25]) could be included but is only included in section 4. Except for section 4, including this effect would complicate the time derivatives because a depends on time and, therefore, η would also depend on time.

The two points of view are incompatible because the equilibrium point of view has a constant pressure throughout the entire tube and no flow while the steady state point of view has a varying pressure along the tube and flow. To merge these two points of view requires further modeling as is described in the remainder of this paragraph. Continue to label the two ends of the tube by 1 and 2. It is assumed that one half of the resistance occurs at end 1 of the tube and one half at end 2, that no volume is stored in the resistive parts of the tube, and that all of the volume is stored between the resistive parts in an infinitesimal length of tube which has no resistance and whatever pressure is implied by the flows through the resistive parts of the tube. With these assumptions, a tube with variable modulus is exactly equivalent to a fragment of an electric circuit which is shown in figure 2(b).

It is important to note that the capacitor in figure 2(b) does not have a capacitance value. Instead, it is labeled by the amount of charge (i.e., fluid volume), denoted by $Q(P,\,\delta_E)$, that it stores. The reason for this is that the capacitor in our model stores charge at zero voltage (i.e., pressure) which is not possible in the standard capacitor in which charge is proportional to voltage. Therefore, the form of Kirchhoff's current law (KCL) at the node labeled by P is figure 2(b) is

$$\frac{P(t) - P_1(t)}{R\left(P(t),\,\delta_E(t)\right)/2} + \frac{P(t) - P_2(t)}{R\left(P(t),\,\delta_E(t)\right)/2} + \frac{\mathrm{d}Q\left(P(t),\,\delta_E(t)\right)}{\mathrm{d}t} = 0, \tag{6}$$

where

$$\frac{\mathrm{d}Q\left(P(t),\,\delta_E(t)\right)}{\mathrm{d}t} = \frac{\partial Q}{\partial P}\left(P(t),\,\delta_E(t)\right)\frac{\mathrm{d}P}{\mathrm{d}t}(t) + \frac{\partial Q}{\partial \delta_E}\left(P(t),\,\delta_E(t)\right)\frac{\mathrm{d}\delta_E}{\mathrm{d}t}(t). \tag{7}$$

Equations (6) and (7) imply a differential equation for P(t) which depends on $P_1(t)$ and $P_2(t)$, specifically,

$$\frac{\mathrm{d}P}{\mathrm{d}t}(t) = -\left[\frac{\partial Q}{\partial P}\left(P(t),\,\delta_E(t)\right)\right]^{-1} \times \left[\frac{\partial Q}{\partial \delta_E}\left(P(t),\,\delta_E(t)\right)\frac{\mathrm{d}\delta_E}{\mathrm{d}t}(t) + \frac{P(t) - P_1(t)}{R\left(P(t),\,\delta_E(t)\right)/2} + \frac{P(t) - P_2(t)}{R\left(P(t),\,\delta_E(t)\right)/2}\right]. \tag{8}$$

Fixed tubes. The fixed tubes (figure 2(a)) have a fixed volume, denoted by Q_a, which is always full and a fixed resistance to flow. Therefore, they are analogous to an electrical resistor of fixed value, denoted by R_a. The fixed

volume, or equivalently charge, Q_a is outside of the electrical circuit model and does not enter the calculations of this paper until equation (11).

2.1.2. Circuit laws. The basic laws are Kirchhoff's current and voltage laws. These laws determine the total flow of hemoglobin through the circuit. In addition, in order to describe pixels which are supplied with blood of variable oxygenation, we desire to describe the fraction of hemoglobin that is oxygenated and to do this we extend Kirchhoff's laws. The primary idea behind the extension is 'well mixing'. In particular, the fraction of HbO_2 supplied by a node is the instantaneous mixing of the fractions of HbO_2 delivered to the node and the fraction of HbO_2 supplied by a capacitor is the integrated mixing of the fractions of HbO_2 delivered to the capacitor in the past. In addition, a further idea is that HbO_2 is converted to HbR in the capacitors.

The extension depends on whether flow is toward a device or node (current is defined as flowing toward the device or node and the value of the current is positive) versus the reverse. For this reason the unit ramp function $r(x)(r(x) = xu(x)$, where $u(x)$ is the unit step function such that $u(x) = 1$ for $x \geqslant 0$ and $= 0$ for $x < 0)$ appears in the equations.

The extensions to Kirchhoff's laws are only described for the limited class of circuit topologies that can be constructed out of sources and the circuit fragments shown in figure 2. Therefore, all capacitors are connected between a node and ground and at most one capacitor is connected per node. Let $Q_\alpha(t)$ and $Q_\alpha^{\mathrm{HbO_2}}(t)$ be the amount of HbT and HbO_2 stored in a capacitor connected between the αth node and ground. Let $f_\alpha(t)$ be the fraction of HbO_2 in the flow away from the αth node. Let $\mathcal{R}_\alpha$ be a set that contains the indices of all resistors attached to node α. For $n \in \mathcal{R}_\alpha$, let $\rho_\alpha(n)$ be the index of the node connected to the α th node via resistor n. Let $\mathcal{C}_\alpha$ and $\chi_\alpha(n)$, $\mathcal{I}_\alpha$ and $\iota_\alpha(n)$, and $\mathcal{V}_\alpha$ and $\upsilon_\alpha(n)$ be the corresponding variables for capacitors, current sources, and voltage sources, respectively. Since at most one capacitor is connected to a node, $\mathcal{C}_\alpha$ is either empty or has a single element which is the ground node.

- A current source resets the fraction of oxygenated hemoglobin to a fixed value f^{I} when it supplies current. Similarly, a voltage source resets the fraction of oxygenated hemoglobin to a fixed value f^{V}. In the application of these tools in this paper, the only source is the left heart, it is described as a voltage source, and the fixed value is 1.0.
- Instantaneous mixing at circuit nodes. The idea is that the fraction of hemoglobin in flow out of a node is the instantaneous average of the fractions of hemoglobin in flow into a node. At every time t (which is not indicated in the equation), there are four possible circuit elements in the branches connected to node α, and the idea of instantaneous mixing is described by the equation

$$f_\alpha = \left(\begin{array}{l} \displaystyle\sum_{n\in\mathcal{R}_\alpha} f_{\rho_\alpha(n)}\, r\left(i^n_{\rho_\alpha(n),\alpha}\right) \\ \quad + \sum_{n\in\mathcal{C}_\alpha} \dfrac{Q_n^{\mathrm{HbO_2}}}{Q_n} r\left(i^n_{\chi_\alpha(n),\alpha}\right) \\ \quad + \sum_{n\in\mathcal{I}_\alpha} f_n^{\mathrm{I}}\, r\left(i^n_{\iota_\alpha(n),\alpha}\right) \\ \quad + \displaystyle\sum_{n\in\mathcal{V}_\alpha} f_n^{\mathrm{V}}\, r\left(i^n_{\upsilon_\alpha(n),\alpha}\right) \end{array} \right) \Bigg/ \left(\begin{array}{l} \displaystyle\sum_{n\in\mathcal{R}_\alpha} r\left(i^n_{\rho_\alpha(n),\alpha}\right) \\ \quad + \sum_{n\in\mathcal{C}_\alpha} r\left(i^n_{\chi_\alpha(n),\alpha}\right) \\ \quad + \sum_{n\in\mathcal{I}_\alpha} r\left(i^n_{\iota_\alpha(n),\alpha}\right) \\ \quad + \sum_{n\in\mathcal{V}_\alpha} r\left(i^n_{\upsilon_\alpha(n),\alpha}\right) \end{array} \right), \tag{9}$$

  where $i^n_{\alpha',\alpha}(t)$ is the current that flows from node α' to node α via circuit element n and the ramp function $r(\,\cdot\,)$ tests the direction of the flow.
- Integrated mixing in capacitors and conversion of HbO_2 to HbR in capacitors. Flows into a capacitor have a fraction of HbO_2 that is determined by the source of the flow, flows out of a capacitor have a fraction of HbO_2 determined by the integrated mixing that occurs in the capacitor, and HbO_2 is converted to HbR in the capacitor. Suppose a capacitor is connected between node α and ground, which is the only configuration that occurs in our vascular models. Then the resulting equation, with the dependence on time suppressed, is

$$\frac{\mathrm{d}Q_\alpha^{\mathrm{HbO_2}}}{\mathrm{d}t} = r\left(i_{\alpha,\mathrm{G}}\right) f_\alpha - r\left(-i_{\alpha,\mathrm{G}}\right) \times \frac{Q_\alpha^{\mathrm{HbO_2}}}{Q_\alpha} - \nu G\left(\frac{Q_\alpha^{\mathrm{HbO_2}}}{Q_\alpha}\right), \tag{10}$$

  where $i_{\alpha,\mathrm{G}}(t)$ is the current the flows from node α to ground and where the term $\nu G\left(Q_\alpha^{\mathrm{HbO_2}}(t)/Q_\alpha(t)\right)$ describes the conversion of HbO_2 to HbR in the capacitor noting that $c_\alpha^{\mathrm{HbO_2}}(t) = Q_\alpha^{\mathrm{HbO_2}}(t)/Q_\alpha(t)$ is the volume fraction of HbO_2 in the capacitor. The conversion term has a constant with units, i.e., ν (units (Volume)/(Time)), multiplying a function, i.e., $G\left(Q_\alpha^{\mathrm{HbO_2}}(t)/Q_\alpha(t)\right)$, and the function G is described in section 2.1.3.
- The value of $Q_\alpha^{\mathrm{HbO_2}}(t)$ determines $Q_\alpha^{\mathrm{HbR}}(t)$ by

$$Q_\alpha^{\mathrm{HbR}}(t) = Q_\alpha(t) - Q_\alpha^{\mathrm{HbO_2}}(t). \tag{11}$$

  When computing the volume of oxygenated, deoxygenated, or total hemoglobin at a pixel (i, j) (denoted by $Q_{i,j}^{\mathrm{HbR}}(t)$, $Q_{i,j}^{\mathrm{HbO_2}}(t)$, and $Q_{i,j}(t)$) rather than in the capacitor at node α (denoted by $Q_\alpha^{\mathrm{HbR}}(t)$, $Q_\alpha^{\mathrm{HbO_2}}(t)$, and $Q_\alpha(t)$), it is necessary to divide the volume in a tube that crosses pixel boundaries between the pixels. In the

calculations reported here, the partitioning is in equal parts.

2.1.3. Conversion of HbO_2 to HbR. A simple description of the conversion of HbO_2 to HbR is used: HbO_2 is converted to HbR plus energy and, because the conversion is enzymatic, it has a limited maximum rate. The description assumes that substrate other than HbO_2 is available in excess. The nonlinear dissociation curve of hemoglobin and molecular oxygen keeps the plasma concentration of molecular oxygen nearly constant. Let the volume fraction of HbO_2 in capacitor α at time t be denoted by $c_\alpha^{HbO_2}(t)$. Let the volume fraction of HbO_2 such that the rate is one-half the maximum rate be denoted by $c_*^{HbO_2}$. Then the Michaelis–Menten rate [26, pp. 192–194] is proportional to the quantity

$$G\left(c_\alpha^{HbO_2}(t)\right) = \frac{c_\alpha^{HbO_2}(t)}{c_*^{HbO_2} + c_\alpha^{HbO_2}(t)} \tag{12}$$

which is a pure number (i.e., no units).

Potentially, the maximum rate, ν (equation (10)) and/or the volume fraction at the half maximal rate, $c_*^{HbO_2}$ (equation (12)), might be controlled. In this paper, ν is controlled but $c_*^{HbO_2}$ is a constant and the control law for ν is described as a part of the neurovascular control component in section 2.2.2.

This model is proposed because the focus of the paper is on oxygenated and deoxygenated hemoglobin and a closed loop control system so the conversion of HbO_2 to HbR and energy is central. Using the lumped-parameter circuit tools, a more detailed model would include the extra-vascular oxygen by connecting the existing circuit to an additional capacitive circuit describing storage and flow of oxygen and conversion of oxygen to energy (which would determine $\delta_{e_{i,j}}^{\uparrow}(t)$ in equation (13)). Because the additional circuit is not directly visible in the OISI data, we have not included the additional circuit in the calculations described in this paper. An additional lumped-parameter circuit is not the most detailed possible model since, if vessel geometry is known in addition to vessel topology, then a distributed-parameter description analogous to the Krogh model [22, section 13.5.1, pp 638ff] could be used.

2.2. Model: neurovascular control component

The neurovascular control component fits between the electrical and vascular components and is essentially a control law. The novelty in the control law is a simple mathematical statement of the metabolic hypothesis applied to oxygen as the metabolite, which could be easily applied to any other metabolite, and a simple connection of the control system to the vascular circuit. The metabolic hypothesis is described in terms of a so-called budget variable that, like the time delay versus a biochemical network described three paragraphs previously, is not physiological but rather is a compact description of the behavior of the physiological system.

Because the components are nonlinear, the neurovascular control component is a model for total signals not perturbations in signals around some baseline signal. Therefore, the neurovascular control component's control law is responsible for homeostasis as well the response to fluctuations, which is the response that is most often measured in experiments.

Our goal is to model optical measurements that are sensitive to HbO_2 and HbR and so oxygenation is an important focus. If desired, other molecules can be given similar focus.

Because the neurovascular control component fits between two other components, the neurovascular control component is constrained in terms of its inputs and outputs which must match those of the other two components. The output of the electrical component is $S(\mathbf{x}, t)$ (equation (24)) which is also the input to the neurovascular control component. In spite of the obvious dependence of the neural activity in the electrical component on sufficient oxygenation, we have not included an output from the neurovascular control component as an input to the electrical component and therefore this model will not describe some pathological conditions. The vascular component has one input from the neurovascular control component which is the Young's modulus of the vessel wall, denoted by $E(t) = E_0 + \delta_{E_{i,j}}(t)$, which therefore must be an output of the neurovascular control component. Due to our focus on oxygenation, the neurovascular control component has one input from the vascular component which is the amount of HbO_2 present in the pixel. Additional inputs from the vascular component could be included if desired.

2.2.1. A feedback controller for homeostasis. A coupling process based on the 'metabolic hypothesis' [7, 27, 28], in particular, a feedback process to achieve energy homeostasis, is described in this section. As is described in section 2.2.3, to achieve homeostasis of some other molecular mediator by feedback would involve the same type of mathematics. At each pixel $[(i, j)]$ there is a time varying $[t]$ homeostasis budget variable denoted by $e_{i,j}(t)$ (units (Unit)) and a target value denoted by by e_* (units (Unit)). The homeostasis budget variable $e_{i,j}(t)$ is at the core of a feedback loop. (1) Suppose $e_{i,j}(t)$ decreases. (2) Then the Young's modulus $E(t) = E_0 + \delta_{E_{i,j}}(t)$ in the vascular component decreases so that the vessel wall becomes more floppy and therefore the vessel dilates. (3) Vessel dilation brings additional blood to the pixel and therefore additional HbO_2 which is converted into HbR in order to create energy thereby increasing $e_{i,j}(t)$. Optionally, the conversion process itself could also be made more efficient which would also increase $e_{i,j}(t)$.

The mathematics to implement this feedback loop has two key components which are equations for the time variation of $e_{i,j}(t)$ and $E(t) = E_0 + \delta_{E_{i,j}}(t)$. The equation for $e_{i,j}(t)$ is a first-order differential equation saying that the rate of change of $e_{i,j}(t)$ with respect to time is the difference between production and consumption. Specifically, the

equation is

$$\frac{\mathrm{d}e_{i,j}}{\mathrm{d}t}(t) = \delta^{\uparrow}_{e_{i,j}}(t) - \delta^{\downarrow}_{e_{i,j}}(t), \tag{13}$$

where $\delta^{\uparrow}_{e_{i,j}}(t)$ is production and $\delta^{\downarrow}_{e_{i,j}}(t)$ is consumption.

The production of energy is proportional to the total rate of conversion of HbO_2 to HbR plus energy. The conversion of HbO_2 to HbR is described by the term $\nu G\left(Q_\alpha^{HbO_2}(t)\right)$ of equation (10). The proportionality constant ν, which is the maximal rate, describes conversion of HbO_2 to HbR which has different units and potentially a different efficiency than the conversion of HbO_2 to $e_{i,j}(t)$. Therefore, a different proportionality constant, which is denoted by ν_b' (units (Unit)/(Time)) and describes the efficiency of the conversion of HbO_2 (and other substrates which are assumed to be in excess) into energy is needed. Therefore, the production of energy based on the HbO_2 in the αth capacitor is

$$\delta^{\uparrow}_{e_{i,j}}(t) = \nu_b' G\left(Q_\alpha^{HbO_2}(t)\right). \tag{14}$$

The consumption of energy is proportional to the power dissipated in the corresponding pixel of the electrical component plus a term for basal metabolism denoted by $\delta^{\downarrow}_{e_{i,j},0}$. In order to quantify this dissipation, let $p_{i,j}(t)$ (units (Unit)/(Time)) denote the power which is

$$p_{i,j}(t) = S(\mathbf{x}, t)\Delta_x\Delta_y, \tag{15}$$

where $S(\mathbf{x}, t)$ is the output of the electrical layer (equation (24)), Δ_x and Δ_y are the sampling intervals in the x and y directions, and $\mathbf{x} = (i\Delta_x, j\Delta_y)$. The consumption is

$$\delta^{\downarrow}_{e_{i,j}}(t) = \gamma p_{i,j}(t) + \delta^{\downarrow}_{e_{i,j},0}, \tag{16}$$

where γ (pure number) describes the efficiency of the electrical component, that is, how many units of metabolic energy are consumed in order to dissipate one unit of energy in the electrical component. This completes the description of the equation for $e_{i,j}(t)$.

The second key equation in the feedback loop is the equation for Young's modulus $E_{i,j}(t) = E_0 + \delta_{E_{i,j}}(t)$. Because the pressure (voltage) equations depend on the derivative of $\delta_{E_{i,j}}(t)$ with respect to time t (e.g., equation (8)), it is essentially that $\delta_{E_{i,j}}(t)$ be smooth. For that reason, we assume that $E(t)$ obeys a critically-damped second order differential equation where the equation is second order because it is necessary for $\mathrm{d}E/\mathrm{d}t$ to be smooth (equation (8)). The driving term for the differential equation and the single time constant of the differential equation differ depending on whether the budget variable $e_{i,j}(t)$ is above or below its threshold. When above threshold, there is a time constant τ_c for constriction of vessels and the steady state value of the Young's modulus is E_0. When below threshold there is a time constant τ_d for dilation and the steady state value of the Young's modulus is αE_0. In mathematical form,

$$\tau_c^2\frac{\mathrm{d}^2E_{i,j}}{\mathrm{d}t^2} + 2\tau_c\frac{\mathrm{d}E_{i,j}}{\mathrm{d}t} + E_{i,j} = E_0 \quad \text{if } e_{i,j} \geqslant e_*, \tag{17}$$

$$\tau_d^2\frac{\mathrm{d}^2E_{i,j}}{\mathrm{d}t^2} + 2\tau_d\frac{\mathrm{d}E_{i,j}}{\mathrm{d}t} + E_{i,j} = \alpha E_0 \quad \text{if } e_{i,j} < e_*. \tag{18}$$

Since $E_{i,j}(t) = E_0 + \delta_{E_{i,j}}(t)$ and E_0 is constant with respect to time, equations (17) and (18) imply that

$$\tau_c^2\frac{\mathrm{d}^2\delta_{E_{i,j}}}{\mathrm{d}t^2} + 2\tau_c\frac{\mathrm{d}\delta_{E_{i,j}}}{\mathrm{d}t} + \delta_{E_{i,j}} = 0 \quad \text{if } e_{i,j} \geqslant e_*, \tag{19}$$

$$\tau_d^2\frac{\mathrm{d}^2\delta_{E_{i,j}}}{\mathrm{d}t^2} + 2\tau_d\frac{\mathrm{d}\delta_{E_{i,j}}}{\mathrm{d}t} + \delta_{E_{i,j}} = (\alpha - 1)E_0 \quad \text{if } e_{i,j} < e_*. \tag{20}$$

The equations presented in this paper concern the case where a budget is either above (desirable) or below (undesirable) a threshold. However, it might be the case that it is desirable to keep the budget between two thresholds rather than above a single threshold. This can be done by generalizing equations (19) and (20) to have three rather than two cases.

2.2.2. Control of ν. A controller for the maximal rate of conversion of HbO_2 to HbR, i.e., ν, is described in this section. The nominal value of ν and the value of $c_*^{HbO_2}$ (equation (12)) are set such that the system extracts a physiologically appropriate fraction of oxygen. In the figure captions, this fraction is referred to as $\mu_0^{HbO_2}/\mu_0^{HbT}$ and can be computed from the data in [29, figure 6]. The nominal value of ν, denoted by ν_b, is then scaled by the output of a control law using the same ideas as were used in section 2.2.1. In particular,

$$\tau_\nu^2\frac{\mathrm{d}^2s_{i,j}}{\mathrm{d}t^2} + 2\tau_\nu\frac{\mathrm{d}s_{i,j}}{\mathrm{d}t} + s_{i,j} = 1 \quad \text{if } e_{i,j} \geqslant e_*, \tag{21}$$

$$\tau_\nu^2\frac{\mathrm{d}^2s_{i,j}}{\mathrm{d}t^2} + 2\tau_\nu\frac{\mathrm{d}s_{i,j}}{\mathrm{d}t} + s_{i,j} = \beta \quad \text{if } e_{i,j} < e_* \tag{22}$$

and $\nu_{i,j} = s_{i,j}\nu_b$.

2.2.3. Alternative feedback controllers. In order to describe the optical measurements, this paper has a detailed description of HbO_2 and HbR and the description includes the idea of an homeostasis budget which controls the conversion of HbO_2 to HbR. As described in section 2.2.1, the same homeostasis budget can control the Young's modulus which controls the vascular component. But that is not necessary. If feedback still exists, then there is some other molecule X and its metabolite X' which are delivered by the vascular system and a budget related to X denoted by $e_{i,j}^X(t)$ with a target value denoted by e_*^X. Then, depending on whether $e_{i,j}^X(t) > e_*^X$ or $e_{i,j}^X(t) \leqslant e_*^X$, the neurovascular control component sets the new value of the perturbation $\delta_{E_{i,j}}(t)$ in the Young's modulus. The methods of this paper can be directly applied to this case. First, in order to include X and X', the approach for HbO_2 and HbR of sections 2.1.2 and 2.1.3 is duplicated for X and X'. Second, the differential equation for the homeostasis budget

(equation (13)) is duplicated for the X budget, specifically,

$$\frac{\mathrm{d}e_{i,j}^{X}}{\mathrm{d}t}(t) = \delta_{e_{i,j}^{X}}^{\uparrow}(t) - \delta_{e_{i,j}^{X}}^{\downarrow}(t), \tag{23}$$

where $\delta_{e_{i,j}^{X}}^{\uparrow}(t)$ is the increase in $e_{i,j}^{X}(t)$ due to the vascular system bringing new X to the (i, j)th pixel and $\delta_{e_{i,j}^{X}}^{\downarrow}(t)$ is the decrease in $e_{i,j}^{X}(t)$ due to the electrical activity described by $S(\mathbf{x}, t)$ (equation (24)). Third, the relationship between $e_{i,j}^{X}(t)$ and $\delta_{E_{i,j}}(t)$ must be defined and the ideas of section 2.2.1 can be used unaltered. Therefore, as soon as X is decided upon and the decrease in the X budget due to electrical activity, i.e., $\delta_{e_{i,j}^{X}}^{\downarrow}(t)$, is determined, the new model is determined. The difference between depletion of a desired quantity and buildup of an undesired quantity is whether $\delta_{e_{i,j}^{X}}^{\downarrow}(t)$ is positive or negative and whether $e_{i,j}^{X}(t) > e_{*}^{X}$ causes decrease in the Young's modulus (leading to dilation) or increase in the Young's modulus (leading to constriction).

If more than one budget contributes to the control of the Young's modulus then the simplest situation is if the control law is a linear combination of effects from the different budgets. The linear combination could occur at the budget variables. Alternatively, the linear combination could occur after the budget variables are transformed into perturbations $\delta_{E_{i,j}}(t)$ on the Young's modulus. In the later case each perturbation could be generated using the ideas of section 2.2.1 with time constants unique to that perturbation. Finally, and most generally, the transformation from budgets to the total perturbation $\delta_{E_{i,j}}(t)$ on the Young's modulus could be a general multiple-input single-output linear dynamical system with the budgets as input.

2.3. Model: electrical component

The paper is focused on the vascular and neurovascular control system components. However, to provide a complete system from electrical excitation to optical measurement, an electrical component is also provided. The electrical component describes the wave propagation velocity and whether superposition of two inputs is sublinear versus supralinear.

Suppose that there are multiple concurrent stimulations, in particular, let $s(\mathbf{x}, t)$ be the stimulation at position $\mathbf{x}$ and time t. The electrical component combines these stimulations to determine the total stimulation of the pixel at location $\mathbf{x}$ at time t (denoted by $S(\mathbf{x}, t)$) by including a spatial oscillation and decay factor z, a propagation speed c, and a potentially nonlinear superposition parameterized by the value of p according to the equation

$$S(\mathbf{x}, t) = \left[\int_{\mathbf{x}'\in\mathbb{R}^2} \left|\Re\left\{\exp\left(z\,\|\mathbf{x}-\mathbf{x}'\|_2\right)\right\} \times\ s\left(\mathbf{x}', t-\|\mathbf{x}-\mathbf{x}'\|_2/c\right)\right|^{p} \mathrm{d}^2\mathbf{x}'\right]^{1/p}, \tag{24}$$

where z is a complex constant, $\Re\{\,\cdot\,\}$ is the real part operation, and $\|\cdot\|_2$ is the euclidean norm. if $z = 1/\lambda$ and λ is real and negative then this equation represents exponential decay with space constant $-\lambda$. if $z = 1/\lambda + \sqrt{-1}/\lambda'$ and λ is real and negative and λ' is real and positive then this equation represents and oscillatory exponential decay with space constant $-\lambda$ for decay and period λ' for oscillation. double stimulus experiments are considered in section 3 in which case

$$s(\mathbf{x}, t) = s_1(t)\delta(\mathbf{x}-\mathbf{x}_1) + s_2(t)\delta(\mathbf{x}-\mathbf{x}_2), \tag{25}$$

where $\delta(\,\cdot\,)$ is the Dirac delta-function in 2D. In this case,

$$S(\mathbf{x}, t) = \left[\sum_{i\in\{1,2\}} \left|\Re\left\{\exp\left(z\,\|\mathbf{x}-\mathbf{x}_i\|_2\right)\right\} \times\ s_i\left(t-\|\mathbf{x}-\mathbf{x}_i\|_2/c\right)\right|^{p}\right]^{1/p}. \tag{26}$$

In order to better understand the role of p, consider the case where the two stimuli are identical, $z = 0$, and $c = \infty$. Then

$$S(\mathbf{x}, t) = \left[2\,\left|s_1(t)\right|^{p}\right]^{1/p} = 2^{1/p}\,|s_1(t)|. \tag{27}$$

For $\infty > p > 1$ the superposition is sublinear since $2^{1/p} < 2$, for $p = 1$ the superposition is linear since $2^{1/1} = 2$, and for $1 > p > 0$ the superposition is supralinear since $2^{1/p} > 2$.

2.4. Model: optical component

The paper is focused on the vascular and neurovascular control system components. However, to provide a complete system from electrical excitation to optical measurement, an optical component are also described which is an application of the Beer–Lambert law.

Many investigators report masses or concentrations of HbO_2 and HbR, which are the output of the vascular component of the model rather than the absorption spectra of light at each pixel. If, however, the absorption results are desired, the key tool is the Beer–Lambert law which describes absorption of light. Since the cortical material is scattering, a portion of the light illuminating the cortex, after a path of length b through the cortex during which absorption occurs, is reradiated from the surface of the cortex and measured. This application of Beer–Lambert involves two types of scatterers, HbO_2 and HbR, and therefore two absorption cross sections σ^{HbO_2} and σ^{HbR}. Let I_0 be the incident radiation intensity and I be the re-radiated radiation intensity. The Beer–Lambert law for two types of scatterers is

$$I(\lambda) = I_0(\lambda)\exp\left(-\left[\sigma^{HbO_2}(\lambda)N^{HbO_2} + \sigma^{HbR}(\lambda)N^{HbR}\right]b(\lambda)\right), \tag{28}$$

where N^{HbO_2} and N^{HbR} are the number of particles of HbO_2 and HbR, respectively, present per unit volume in the volume through which the beam propagates and path length, both cross sections, and both intensities depend on the wavelength λ. In section 2.2, μ^{HbO_2} and μ^{HbR} are defined to be the mass of HbO_2 and HbR, respectively, in a pixel and $\bar{\mu}^{HbO_2}$ and $\bar{\mu}^{HbR}$ are the corresponding values after incorporating the effect of the point spread function. Effectively add the missing third dimension of the model by assuming that the pixel has third dimension Δ_z. Then $N^{HbO_2} = \bar{\mu}^{HbO_2}/(w^{HbO_2}\Delta_x\Delta_y\Delta_z)$ and

$N^{\mathrm{HbR}} = \bar{\mu}^{\mathrm{HbR}} / (w^{\mathrm{HbR}} \Delta_x \Delta_y \Delta_z)$, where $w^{\mathrm{HbO_2}}(w^{\mathrm{HbR}})$ converts $\bar{\mu}^{\mathrm{HbO_2}}(\bar{\mu}^{\mathrm{HbR}})$ with units of (Mass) to number of molecules which is dimensionless.

3. Results

Much OISI data is published in terms of the time-course of hemoglobin concentrations, often at a single location. Therefore, it is possible to compare with the published OISI data without including in the model a description of the relationship between cerebral blood flow and volume with the resulting optical signals. In addition, when only a single location is considered, the model is further simplified to a model of a single pixel which implies that no electrical layer is included. The predictions of the mathematical model are computed by a program (available from the authors) written in the Matlab programming language [30].

In both OISI and fMRI experiments, the resulting electrical signal in the cortex is not known. For this reason, some of the signals in our model have an arbitrary unit which is denoted by '(Unit)'. This unit eventually cancels when computing quantities of interest such as μ^{HbT}. In the neurovascular control component of the model, we use signed contributions to the homeostasis budget so that e_*, the target value for the homeostasis budget (section 2.2.1, equations (17) and (18)) can be taken to be zero which needs no unit. Also in the neurovascular control component of the model, the Michaelis–Menten conversion of HbO_2 to HbR and energy has the same arbitrary unit for the energy.

Although it is not fundamental to our modeling approach, in this paper we assume that the hematocrit is constant. Therefore, in some standard volume, the sum of the masses of oxygenated and deoxygenated hemoglobin ($\mu^{\mathrm{HbO_2}} + \mu^{\mathrm{HbR}}$) is constant; the sum of the concentrations ($c^{\mathrm{HbO_2}} + c^{\mathrm{HbR}}$) is constant; and, since hemoglobin only occurs in the two forms, the sum of the fractions ($f^{\mathrm{HbO_2}} + f^{\mathrm{HbR}}$) is one. Because fractions are restricted to the interval from 0 to 1, which is not true for concentrations or masses, the computer program generally uses fractions.

The value of the model is in its ability to represent and also predict experimental data. Using a range of parameters, we demonstrate the use of the model to describe experimental data from several different laboratories in the following sections. The parameter values used are a mix of values from literature and values selected by NRC based on forward simulations of the model. Simple automatic methods of selecting parameters, such as numerical minimization by least squares, are probably not appropriate because small changes in the timing of high-derivative regions lead to large least squares errors. In addition, because of the nonlinear nature of the model, automatic methods would require initial conditions. One natural choice would be the values used here.

3.1. Nominal parameters

The model describes a single pixel and uses the topology shown in figure 3(a). Figures 4(A)–(F) shows the response of the model using a nominal set of parameters. The parameters we have chosen result in a moderate initial dip in the concentration of HbO_2 in these noise-free curves.

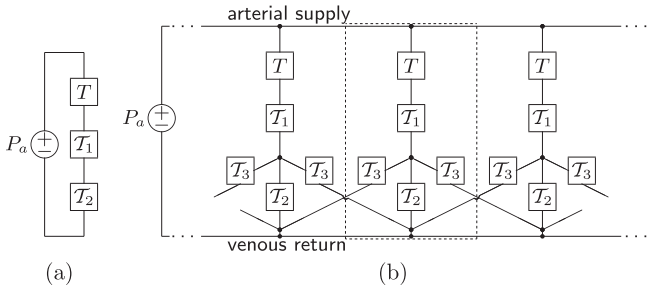

Figure 3. Block diagrams for the numerical calculations. As in figure 2, T indicates a purely resistive component with fixed modulus while $\mathcal{T}$ indicates a component with both resistive and capacitive characteristics and a variable modulus. Conversion of $\mu^{\mathrm{HbO_2}}$ to μ^{HbR} occurs in $\mathcal{T}_2$ and $\mathcal{T}_3$. Panel (a) The block diagram for the one-pixel models. The correspondence between the block diagram and anatomical structures is not perfect, since arteries and arterioles supply oxygen as well as capillaries [38, 39], but roughly T describes the large arterial supply, $\mathcal{T}_1$ describes the small arteriolar supply, and $\mathcal{T}_2$ describes the capillary bed and more distal structures. Panel (b) The block diagram for the many-pixel model with the components corresponding to a single example pixel enclosed by dotted lines. The additional class of block labeled $\mathcal{T}_3$ describes capillaries and more distal structures that originate in one pixel but terminate in a second pixel, thereby delivering partially oxygenated hemoglobin to the second pixel. While only one capillary is shown (e.g., $\mathcal{T}_2$ in panel (a)), the calculations are done with a parallel array of N capillaries.

One feature of interest in the response is the amplitude of the initial dip in the concentration of HbO_2. Figures 4(G)–(H) describes how the initial dip varies as a function of the two most important parameters, β (which controls the maximal rate of conversion of HbO_2 to HbR (equations (21)–(22)) and τ_d (which is the time constant for the change in Young's modulus during dilation (equations (17)–(18))), and demonstrates that the predictions of the model change from no initial dip to an initial dip as large as 0.5%.

The range of parameters that appear in the figures is described in this paragraph. For the neurovascular control component the parameter ranges are $c_*^{\mathrm{HbO_2}} = 0.1$–$0.2$, $e_* = 0$ (Unit), $\nu_b' = 2.61 \times 10^{12}$–$8.27 \times 10^{12}$ (Unit)/s, $\gamma = 1$ [31–34], and $\delta_{e_{i,j},0}^{\downarrow} = 69.58$–$1208.7$ (Unit)/s. For the vascular component the parameter ranges are $a_{a,0} = 20\,\mu$m, $a_{v,0} = 2.5$–$3.0\,\mu$m, $P_{a,0} = 13300$ Pa, $P_{v,0} = 6650$ Pa, $\zeta E_{a,0} = 0.28$–0.37 Nm^{-1}, $\zeta E_{v,0} = 0.017$–0.025 Nm^{-1}, $\eta = 0.005$ Pa s, $l_a = 5$ mm, $l_v = 100$–$500\,\mu$m, $N = 30$–64, $\nu_b = 15.52$–484.90 (Unit)/s, $\tau_d = 0.9$–1.9 s, $\tau_c = 6.8$–1.0 s, $\tau_\nu = 0.15$ s, $\alpha = 0.85$–0.9, $\beta = 1.00$–1.01, and $\mu_0^{\mathrm{HbO_2}} / \mu_0^{\mathrm{HbT}} = 0.30$–$0.35$.

3.2. Description of a fore-paw stimulation experiment

Figure 5 shows the the relative changes in hemoglobin and oxygenation for an example using OISI to measure neurovascular coupling for an example modeled on [35, figure 3] which describes the response in a rat to forepaw stimulation at

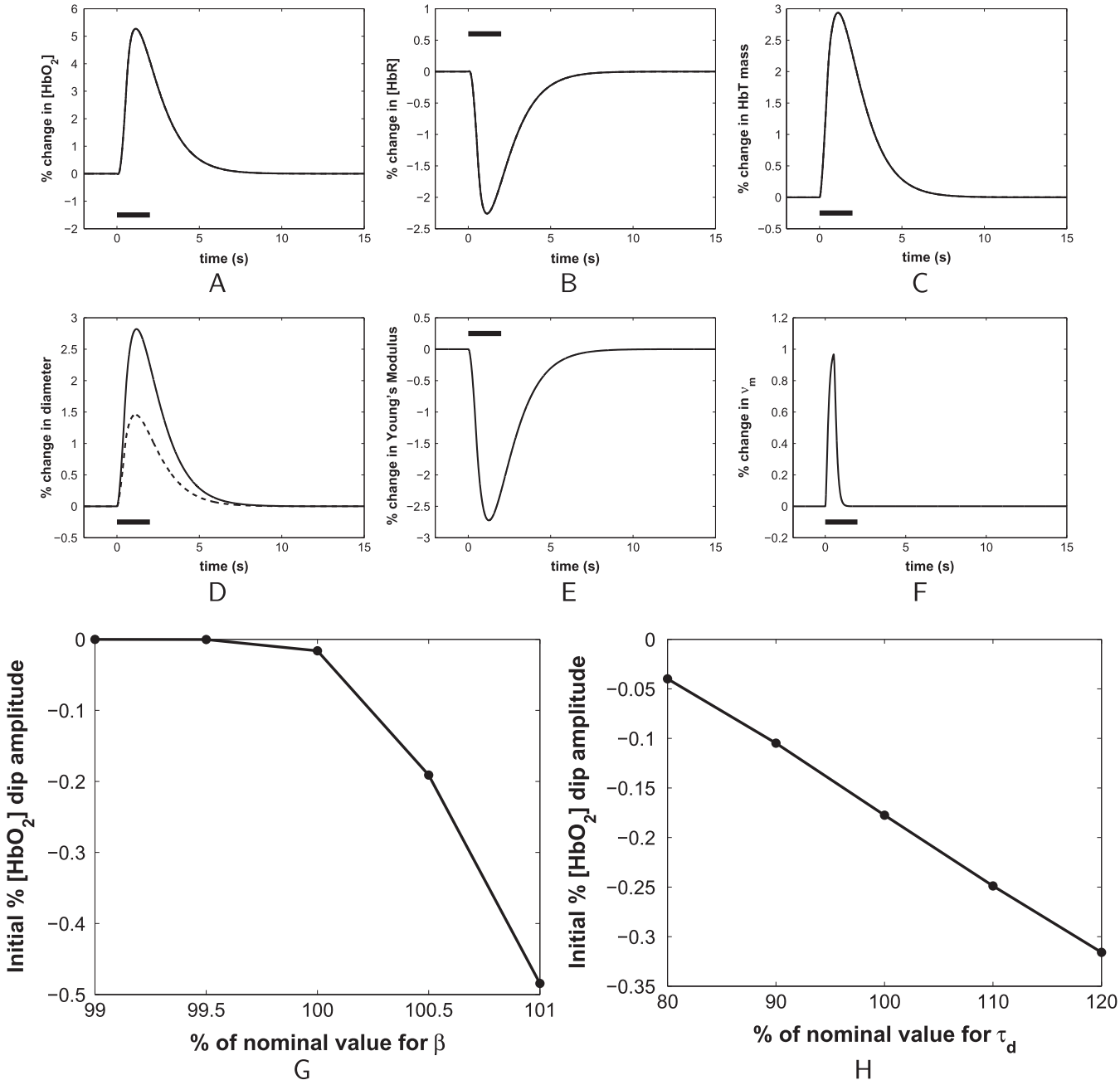

Figure 4. Behavior of the model with nominal parameter values including sensitivity to the parameter values. Behavior of the model is described by the time course (units of seconds) of percentage changes in (A) concentration of oxygenated hemoglobin $(100[(\frac{Q^{\mathrm{HbO2}}(t)}{Q^{\mathrm{HbT}}(t)})/(\frac{Q^{\mathrm{HbO2}}(0)}{Q^{\mathrm{HbT}}(0)}) - 1])$, (B) concentration of deoxygenated hemoglobin $(100[(\frac{Q^{\mathrm{HbR}}(t)}{Q^{\mathrm{HbT}}(t)})/(\frac{Q^{\mathrm{HbR}}(0)}{Q^{\mathrm{HbT}}(0)}) - 1])$, (C) total mass of hemoglobin $(100(\mu^{\mathrm{HbT}}(t)/\mu^{\mathrm{HbT}}(0) - 1))$, (D) arteriolar radius $(100(a(t)/a(0) - 1))$, (E) Young's modulus $(100(E(t)/E(0) - 1))$, and (F) maximum rate of conversion of HbO_2 to HbR $(100(\nu(t)/\nu(0) - 1))$. The bar indicates the duration of the excitation. Sensitivity of the model to the parameter values is described by plotting the initial $[HbO_2]$ dip amplitude as a function of the parameter value where the value is reported as a percent change in the nominal value. (G): sensitivity with variation in β which controls the maximal rate of conversion of HbO_2 to HbR (equations (21)–(22)). (H): sensitivity with variation in τ_d which is the time constant for the change in Young's modulus during dilation (equations (17)–(18)). For the neurovascular control component the parameters are $c_*^{\mathrm{HbO_2}} = 0.2$, $e_* = 0$ (Unit), $\nu_b' = 8.27 \times 10^{12}$ (Unit)/s, $\gamma = 1$ [31–34], and $\delta_{e_{i,j},0}^{\downarrow} = 1208.7$ (Unit)/s, while for the vascular component the parameters are $a_{a,0} = 20\ \mu$m, $a_{v,0} = 2.5\ \mu$m, $P_{a,0} = 13300$ Pa, $P_{v,0} = 6650$ Pa, $\zeta E_{a,0} = 0.37$ N m^{-1}, $\zeta E_{v,0} = 0.17$ N m^{-1}, $\eta = 0.005$ Pa s, $l_a = 5$ mm, $l_v = 100\ \mu$m, $N = 64$, $\nu_b = 484.90$ (Unit)/s, $\tau_d = 1$ s, $\tau_c = 1$ s, $\tau_\nu = 0.15$ s, $\alpha = 0.9$, $\beta = 1.01$, and $\mu_0^{\mathrm{HbO_2}}/\mu_0^{\mathrm{HbT}} = 0.3$. In the absence of the electrical layer, the input to the budget equation (equation (13)) is directly controlled. The excitation ($p(t)$ in equation (16)) lasts 2 s and is a sequence of positive-going pulses where the time interval between the leading edges of sequential pulses is 0.05 s (i.e., 20 Hz).

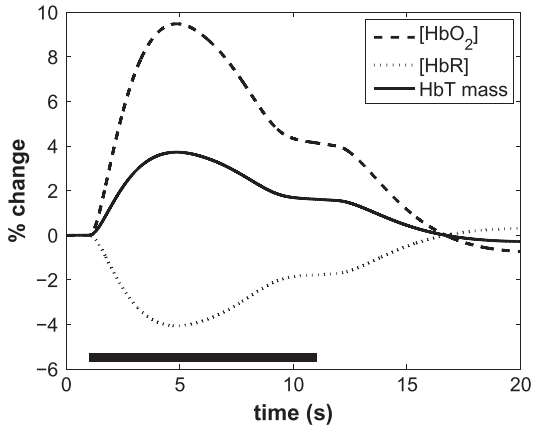

Figure 5. Forepaw stimulation. Simulated trajectories (time unit of seconds) of oxygenated ($100[(\frac{Q^{\mathrm{HbO2}}(t)}{Q^{\mathrm{HbT}}(t)})/(\frac{Q^{\mathrm{HbO2}}(0)}{Q^{\mathrm{HbT}}(0)}) - 1]$), deoxygenated ($100[(\frac{Q^{\mathrm{HbR}}(t)}{Q^{\mathrm{HbT}}(t)})/(\frac{Q^{\mathrm{HbR}}(0)}{Q^{\mathrm{HbT}}(0)}) - 1]$), and total ($100(\mu^{\mathrm{HbT}}(t)/\mu^{\mathrm{HbT}}(0) - 1)$) hemoglobin concentrations (Q ratios) or masses (μ) in response to a 10 s stimulation demonstrating a plateau midway through the response which is similar to experimental data from [35, figure 3] which describes the response in a rat to forepaw stimulation at 3 Hz for 10 s. The bar indicates the duration of the excitation. For the neurovascular control component the parameters are $c_*^{\mathrm{HbO_2}} = 0.1$, $e_* = 0$ (Unit), $\nu_b' = 5.08 \times 10^{12}$ (Unit)/s, $\gamma = 1$ [31–34], and $\delta_{e_{i,j},0}^{\downarrow} = 69.58$ (Unit)/s, while for the vascular component the parameters are $a_{a,0} = 20\ \mu$m, $a_{v,0} = 3\ \mu$m, $P_{a,0} = 13300$ Pa, $P_{v,0} = 6650$ Pa, $\zeta E_{a,0} = 0.28$ N m^{-1}, $\zeta E_{v,0} = 0.025$ Nm^{-1}, $\eta = 0.005$ Pa s, $l_a = 5$ mm, l_v=500 μm, $N = 30$, $\nu_b = 15.52$ (Unit)/s, $\tau_d = 1.9$ s, $\tau_c = 6.8$ s, τ_ν is unneeded since $\beta = 1$, $\alpha = 0.85$, $\beta = 1$, and $\mu_0^{\mathrm{HbO_2}}/\mu_0^{\mathrm{HbT}} = 0.3$. In the absence of the electrical layer, the input to the budget equation (equation (13)) is directly controlled. The excitation ($p(t)$ in equation (16) lasts 10 s and is a sequence of positive-going pulses where the time interval between the leading edges of sequential pulses is (1/3) s (i.e., 3 Hz). The budget ($e(t)$) starts at the threshold e_* and is driven below the threshold by the pulses, which results in dilation.

3 Hz for 10 s. The data is for a single pixel and so the topology shown in figure 3(a) is used. This is a longer duration stimulation than the 2 s duration of the stimulation in figure 4 and therefore the duration of the response is longer. More interestingly, and similar to the experimental data in [35, figure 3], the decay from the peak signals is in two phases with an intermediate plateau. The initial peak in HbO_2 is due to the presence of the temporal derivative of the Young's modulus, i.e., $\mathrm{d}\delta_E/\mathrm{d}t$, in equation (8).

3.3. Description of a whisker-pad stimulation experiment at multiple stimulation frequencies

Single-pixel experimental data show that the relationship between the frequency of whisker stimulation and neurovascular coupling is nonlinear and this behavior is captured by the model described in this paper using the topology of figure 3(a). Figure 6 shows hemoglobin and cerebral blood flow curves for an example modeled on [29, 'awake' panels of figure 6, p 39] which combines OISI and and laser Doppler flowmetry experiments done sequentially [29, p 35, column 1, paragraph 2]. While the example in figure 5 considered an input of long duration, this considers an input of various frequencies, including higher frequencies up to 40 Hz, through a rat whisker pad by electrical stimulation. As in the experimental data, there is a strong frequency dependence in the response amplitude of the model. The whisker representation in the somatosensory cortex of rodents is a favorite system in which to study neurovascular coupling in response to simulation of whisker because it is easy to apply varying temporal and spatial patterns. The evoked neural activity in somatosensory cortex and the neurovascular coupling response to a temporal series of stimulations is not simply the sum of the response to a single stimulation with appropriate delays. Changing the frequency or number of stimulation events results in nonlinear response in blood flow and oxygenation dynamics. Figure 6 demonstrates that model parameters can be chosen such that the model's predictions and the experimentally observed signals are similar.

3.4. Demonstration of the nonlinear response to multiple simultaneous stimulations at one location

When the neurovascular system receives multiple stimuli at the same time and location, the total response of the system is not the sum of the responses to each of the stimuli when presented as an isolated stimulus. Figure 7 demonstrates this effect (a nonlinear superposition effect) with two examples both in single-pixel circumstances using the topology of figure 3(a). The inputs are the summation of two signals of different amplitudes or of different frequencies. Both the actual output of the model and the linear superposition of the individual outputs that occur when the two stimulus signals are presented separately are shown. The actual outputs are substantially smaller in amplitude than the linear superpositions of the individual outputs thereby demonstrating the nonlinear superposition effect.

3.5. Response to multiple stimuli in different locations

Much of the quantitative published data concerns the response at a single point, i.e., a single pixel, to a stimulus at a single point, e.g., a whisker stimulation. However, a common use of OISI and fMRI is to infer the spatial location of the neuronal activity due to a stimulation. For instance, the rodent whisker system is used to study the spatial relationship between signal generated by stimulating different combination of whiskers. As in the temporal super position of whisker deflections (section 3.4), the stimulation of multiple whiskers at the same time also does not result in neural or vascular responses that can be predicted by a summation of the response to a single whisker with appropriate spatial translations. The model presented in this paper describes a 2D array of pixels responding to a 2D input signal. The multi-pixel topology of figure 3(b) is used. In figure 8 we show the 2D response of the model as an image at various times in response to a single spatially-restricted stimulation and in response to a pair of spatially-restricted stimulations. The major point is the model's prediction of a sublinear superposition of the responses to the pair of stimuli.

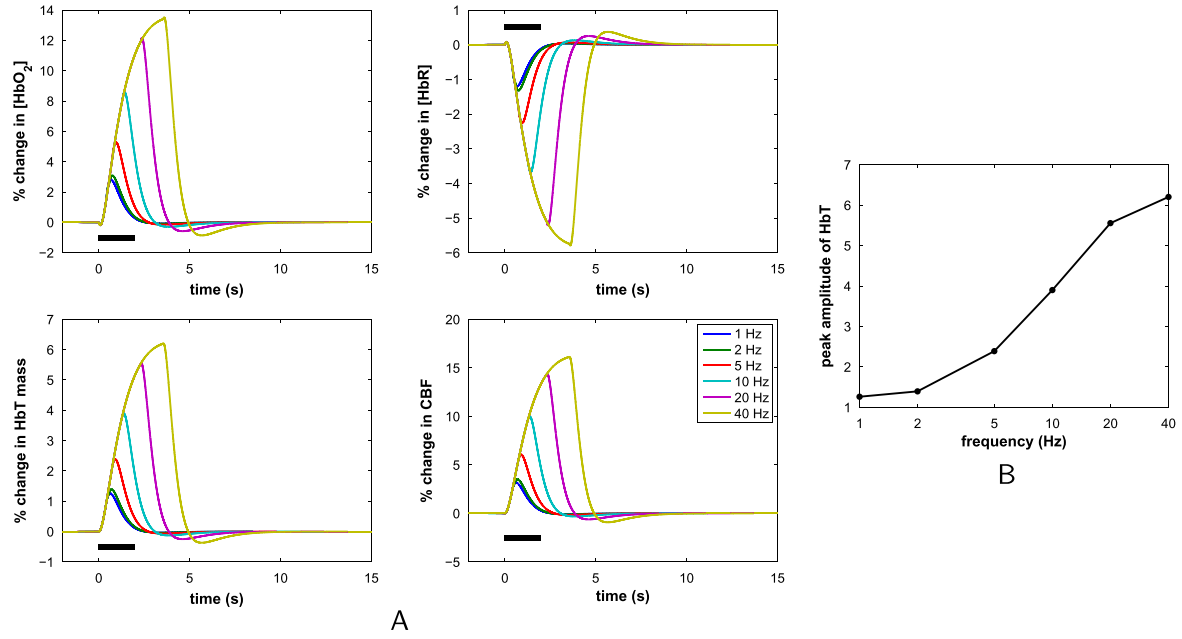

Figure 6. Whisker pad stimulation. (A): simulated trajectories (time unit of seconds) of oxygenated $(100[(\frac{Q^{\mathrm{HbO_2}}(t)}{Q^{\mathrm{HbT}}(t)})/(\frac{Q^{\mathrm{HbO_2}}(0)}{Q^{\mathrm{HbT}}(0)}) - 1])$, deoxygenated $(100[(\frac{Q^{\mathrm{HbR}}(t)}{Q^{\mathrm{HbT}}(t)})/(\frac{Q^{\mathrm{HbR}}(0)}{Q^{\mathrm{HbT}}(0)}) - 1])$, and total $(100(\mu^{\mathrm{HbT}}(t)/\mu^{\mathrm{HbT}}(0) - 1))$ hemoglobin concentrations (Q ratios) or masses (μ) and cerebral blood flow $(100(\mathrm{CBF}(t)/\mathrm{CBF}(0) - 1))$ in response to a stimulations of varying frequencies which are similar to experimental data from [29, 'awake' panels of figure 6, p 39] which describes the response in a rat to electrical stimulation of a whisker pad at 1–40 Hz for 2 s. In [29], the OISI and and laser Doppler flowmetry experiments were performed sequentially [29, p. 35, column 1, paragraph 2]. In order of increasing amplitudes, the curves are for stimuli at 1, 2, 5, 10, 20, or 40 Hz. The bar indicates the duration of the excitation. (B): plot of peak amplitude of total hemoglobin mass $(100(\mu^{\mathrm{HbT}}(t)/\mu^{\mathrm{HbT}}(0) - 1))$ in (A) versus frequency. For the neurovascular control component the parameters are $c_*^{\mathrm{HbO_2}} = 0.08$, $e_* = 0$ (Unit), $\nu_b' = 5.0 \times 10^{12}$ (Unit)/s, $\gamma = 1$ [31–34], and $\delta^{\downarrow}_{e_{i,j},0} = 353.42$ (Unit)/s, while for the vascular component the parameters are $a_{a,0} = 20\ \mu$m, $a_{v,0} = 2.5\ \mu$m, $P_{a,0} = 13300$ Pa, $P_{v,0} = 6650$ Pa, $\zeta E_{a,0} = 0.37\ \mathrm{Nm}^{-1}$, $\zeta E_{v,0} = 0.017\ \mathrm{Nm}^{-1}$, $\eta = 0.005$ Pa s, $l_a = 10$ mm, $l_v = 30\ \mu$m, $N = 64$, $\nu_b = 40.95$ (Unit)/s, $\tau_d = 1.2$ s, $\tau_c = 0.8$ s, $\tau_v 0.15$ s, $\alpha = 0.9$, $\beta = 1.005$, and $\mu_0^{\mathrm{HbO_2}}/\mu_0^{\mathrm{HbT}} = 0.3$. In the absence of the electrical layer, the input to the budget equation (equation 13) is directly controlled. The excitation ($p(t)$ in equation (16)) lasts 2 s and is a sequence of positive-going pulses where the time interval between the leading edges of sequential pulses is 1, 0.5, 0.2, 0.1, 0.05, or 0.025 s (i.e., 1, 2, 5, 10, 20, or 40 Hz) in the six different curves. The budget ($e(t)$) starts at the threshold e_* and is driven below the threshold by the pulses, which results in dilation.

4. Grubb's law

As demonstrated in section 3, the model can fit experimental data. However, it can also describe more abstract relationships. In particular, the model predicts a relationship between cerebral blood volume and flow in the steady state. In this section we compute that relationship and compare it with Grubb's law [19] which was first described in 1974 based on radiotracer experiments in rhesus monkeys.

Denote cerebral blood volume by CBV and cerebral blood flow by CBF. Grubb's law [19, equation 5, p 631] is the relationship

$$\mathrm{CBV}/\mathrm{CBV}_0 = 0.8\big(\mathrm{CBF}/\mathrm{CBF}_0\big)^{0.38}, \tag{29}$$

where, in the units of [19, equation 5, p 631] (CBV in milliliters of blood per 100 gm and CBF in milliliters of blood per 100 gm per minute), the constants CBV_0 and CBF_0 have numerical value 1.

The model described in this manuscript includes temporal and spatial dynamics which are not present in Grubb's law. Therefore, to connect between the model and Grubb's law we assume that the model is spatially homogeneous and in the steady state. The detailed vascular topology is not known, so we use the topology of figure 3(b). Spatial homogeneity implies that the flows between pixels via $\mathcal{T}_3$ in figure 3(b) are zero. Furthermore, Grubb's law comes from imaging studies with voxels that are large compared to the length of a capillary so that, even in an inhomogeneous situation, the flow between pixels is small. Being in the steady state implies that the capacitors are open circuit. Therefore the entire behavior of the model is determined by the serial connection of the five resistors $R^{(a)}$, $R(P_{i,j}^{(a)}(t), \delta_{E_{i,j}}(t))/2$, $R(P_{i,j}^{(a)}(t), \delta_{E_{i,j}}(t))/2$, $R(P_{i,j}^{(v)}(t), \delta_{E_{i,j}}(t))/2$, and $R(P_{i,j}^{(v)}(t), \delta_{E_{i,j}}(t))/2$ between P_a and ground in the path T, $\mathcal{T}_1$, and $\mathcal{T}_2$ of figure 3(b) after the electrical circuits of figure 2 are inserted into figure 3(b). CBF is then the ratio of P_a divided by the sum of these five resistors. The voltages at the four nodes between the five resistors can all be computed by voltage divider calculations. Since no current flows through the resistors in $\mathcal{T}_3$ in figure 3(b), it follows that $P_{i,j}^{(R)}(t) = P_{i,j}^{(0)}(t)$. From the voltages $P_{i,j}^{(a)}(t)$, $P_{i,j}^{(v)}(t)$,and $P_{i,j}^{(R)}(t)$, the charges $Q(P_{i,j}^{(a)}(t)$,

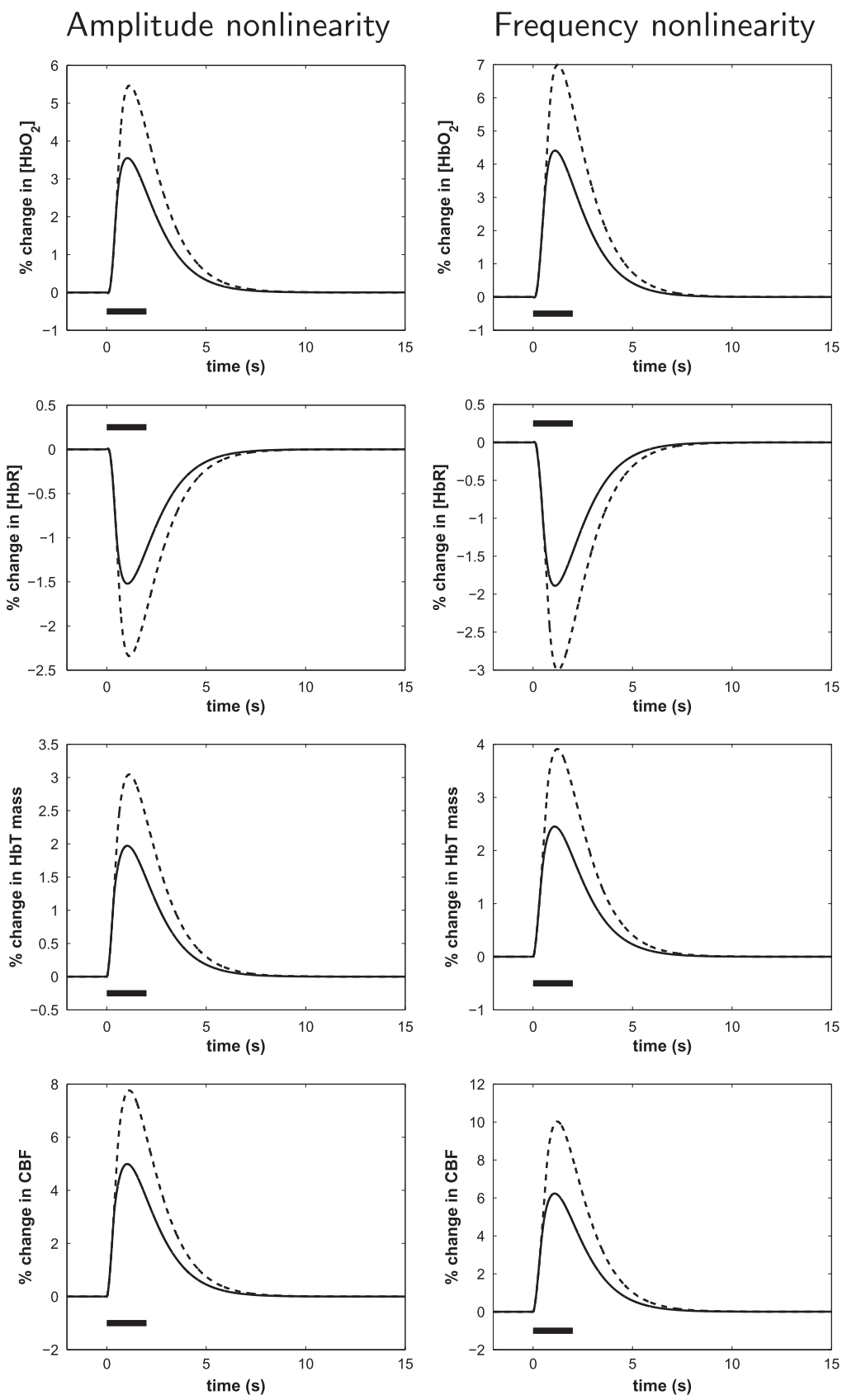

Figure 7. Nonlinearity with respect to amplitude and frequency of the excitation signals based on the model of figure 4 with the excitations of figure 6. The solid curves show the response of the system when excited by the sum of two excitations while the dotted curves show the sum of the responses to the individual excitations. The excitations for the amplitude example in the left column are both the 10 Hz excitation from figure 6 so the double excitation is the same as either single excitation with an amplitude scaled by a factor of 2. The excitations for the frequency example in the right column are the 10 and 20 Hz excitations of figure 6. The bar indicates the duration of the excitation.

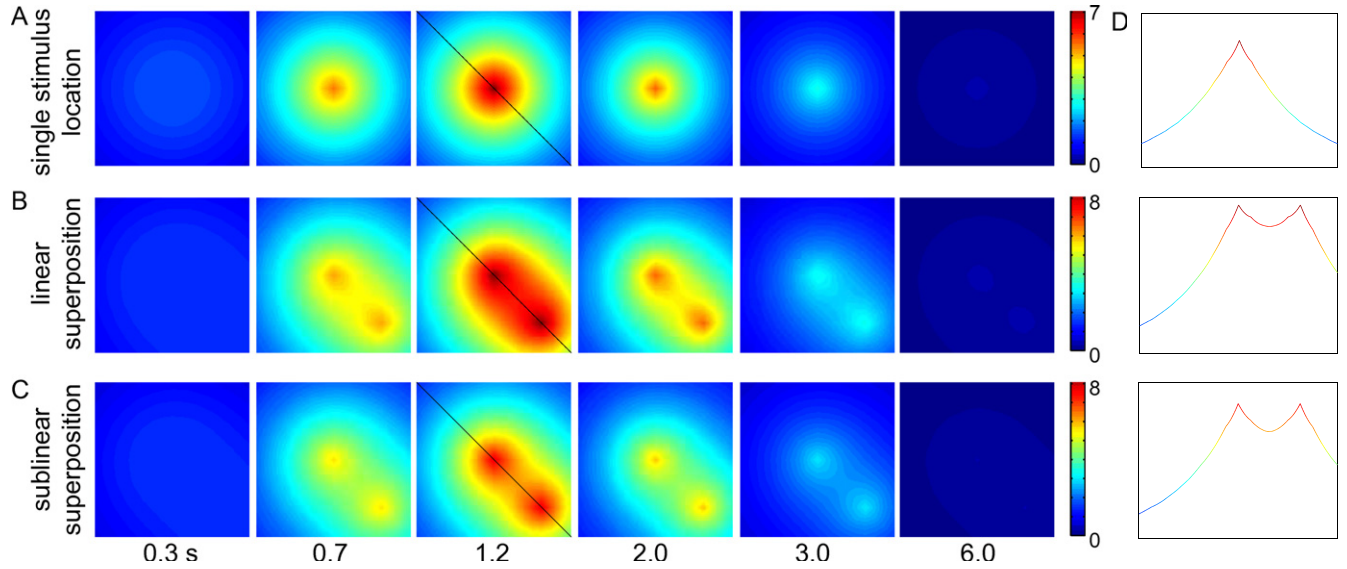

Figure 8. Demonstration that the response to multiple stimuli is a nonlinear function of the stimuli. Images from the response of the 2D model at the indicated times (units of seconds) and a plot of the response along the line drawn in the 1.2 or 1.24 s image. If the response to multiple stimuli was linear then the response would be as is shown in (B) while the actual response is shown in (C). The parameters are the nominal parameters of figure 4 with the additional parameters (equation (24)) of $c = \infty$ $z = 4$ (Pixel)$^{-1}$, and $p = 1.6$ except for (B), where $p = 1$. The temporal characteristics of the input are unchanged from the input of figure 4 and the pulse amplitude is 5. The same color map is used in all images of (A) and in all images of (B) and (C). Plots showing the response along the inter-peak line in the 1.2 s and the two 1.24 s images, which are the images with the maximal response, are displayed in (D).

$\delta_{E_{i,j}}(t))$, $Q(P_{i,j}^{(v)}(t), \delta_{E_{i,j}}(t))$, and $Q(P_{i,j}^{(R)}(t), \delta_{E_{i,j}}(t))$ can be computed and the sum of these charges is CBV. Since there is no time dependence, the '(t)' can be removed and since there is no spatial dependence the '$_{i,j}$' can be removed.

Rather than using the circuit ideas of section 2.1, outlined in the previous paragraph, to derive the equivalent of Grubb's law for the model described in this manuscript, the underlying tube ideas of sections 2.1.1 and 2.1.1 are used. The contribution of $Q(P^{(a)}, \delta_E)$, corresponding to arterioles, is ignored since it is much smaller than the contribution from capillaries. The two contributions from capillaries, $Q(P^{(v)}, \delta_E)$ and $Q(P^{(R)}, \delta_E)$, are combined in terms of a total length l_c of capillaries. In the tube approach, if the length of the tube is l_c and the radius of the tube is a_c then

$$\text{CBV} = l_c \pi a_c^2. \tag{30}$$

Furthermore, if the pressure from end-to-end of the tube is P_c and the resistance to flow through the tube is R_c then

$$\text{CBF} = \frac{P_c}{R_c} = \frac{P_c}{8\eta l_c \Big/ \left[\pi a_c^4\right]} = \frac{\pi P_c}{8\eta l_c} a_c^4, \tag{31}$$

where the second equality is due to Poiseuille's formula (equation (4)). Solving equation (31) for a_c^2 and using the result in equation (30) gives

$$\text{CBV} = l_c \pi \sqrt{\text{CBF}\frac{8\eta l_c}{\pi P_c}} = l_c \sqrt{\frac{8\pi\eta l_c}{P_c}}\,\text{CBF}^{0.5} \tag{32}$$

which is the equivalent of Grubb's law for the model described in this paper.

A more sophisticated resistance formula than Poiseuille's formula (equation (4)) would alter the a_c^4 term in equation (31) which would alter the 0.5 exponent in equation (32). Therefore it may be possible to move the exponent closer to the value in [19, equation 5, p 631]. An alternative point of view is that viscosity η depends on radius a_c via a power law with unknown exponent, i.e., $\eta = \eta_0 a_c^{2\omega}$ for some value of ω [24, 25], and use Grubb's law to estimate ω. With this point of view, equation (31) becomes

$$\text{CBF} = \frac{P_c}{8\eta_0 a_c^{2\omega} l_c \Big/ \left[\pi a_c^4\right]} = \frac{\pi P_c}{8\eta_0 l_c} a_c^{2(2-\omega)} \tag{33}$$

resulting in

$$a_c^2 = \left(\text{CBF}\frac{8\eta_0 l_c}{\pi P_c}\right)^{1/(2-\omega)} \tag{34}$$

which implies that

$$\begin{aligned}\text{CBV} &= l_c \pi \left(\text{CBF}\frac{8\eta_0 l_c}{\pi P_c}\right)^{1/(2-\omega)} \\ &= l_c \pi \left(\frac{8\eta_0 l_c}{\pi P_c}\right)^{1/(2-\omega)} \text{CBF}^{1/(2-\omega)}.\end{aligned} \tag{35}$$

In order to match the exponent value of 0.38 in [19, equation 5, p 631], it is necessary to have $1/(2-\omega) = 0.38$ which implies that $\omega = -0.63$.

P_c can be expressed in terms of P_a and the fundamental properties of tubes, specifically, E_0, δ_E, a_0, t, and l, and the fundamental property of blood, specifically, η. First solve a two-component vector fixed-point equation constructed from

two voltage divider formulas, specifically,

$$P^{(a)} = P_a \frac{R\left(P^{(a)}, \delta_E\right)/2 + R\left(P^{(v)}, \delta_E\right)}{R^{(a)} + R\left(P^{(a)}, \delta_E\right) + R\left(P^{(v)}, \delta_E\right)}, \tag{36}$$

$$P^{(v)} = P_a \frac{R\left(P^{(v)}, \delta_E\right)/2}{R^{(a)} + R\left(P^{(a)}, \delta_E\right) + R\left(P^{(v)}, \delta_E\right)}, \tag{37}$$

where $R(P, \delta_E)$ is defined by equation (5) and the solution for $P^{(a)}$ and $P^{(v)}$ is denoted by $P_*^{(a)}$ and $P_*^{(v)}$, respectively. If the constant $R^{(a)}$ is also expressed in terms of the diameter of the arteriole by Poiseuille's formula then the constant η is not needed because it occurs in every resistance term and therefore cancels from the ratios. Then $P_c = 2P_*^{(v)}$. Using this value for P_c gives the constant for equation (32) in terms of system blood pressure P_a.

5. Discussion

In this paper we present a set of tools for modeling the cerebral microvasculature and demonstrate a complete model that can be used to evaluate and predict experimental signals such as those generated in imaging modalities such as OISI. Important goals that have been achieved are to describe both blood flow and cerebral blood volume, leading to use of both resistors and capacitors; to include the possibility that blood moves across the imaging field so that models of neurovascular coupling must include the possibility that the blood flow might enter the microvasculature in one pixel but exit from a different pixel; and to describe the flows and volumes of both oxygenated hemoglobin and deoxygenated hemoglobin and the conversion of oxygenated into deoxygenated hemoglobin. Part of the model is closely based on physical principles, such as Kirchhoff's current and voltage laws, and Laplace's and Poiseuille's laws, while other parts are phenomenological, such as control laws. As demonstrated in section 3, changing the parameters in the complete model leads to quite different behaviors, e.g., the presence or absence of an initial decrease in HbO_2 in response to an excitation. Finally, in section 4, the model is connected to the macroscopic world by deriving Grubb's law from the model.

Because the model is motivated by human neurosurgery applications, the goal is an approach that is sufficiently simple such that the parameters in the model can be determined for individual subjects, e.g., for intra-operative clinical video [6] from a patient, rather than for populations of subjects. Determining a model from data originating in a single subject limits the complexity of the model. For instance, the ethanol pharmacokinetic models of [36] represent an entire human's pharmacokinetic response to infused ethanol by as few as two differential equations. However, in spite of the great simplification, these models have proven useful in clinical research because all parameters can be determined from limited data recorded from a individual subject. For instance, such a pharmacokinetic model individualized to a particular person allows computation of a time-varying intravenous ethanol infusion for that person that achieves a pre-specified time-varying brain ethanol exposure. Similarly, such an individualized model allows computation of infusions that are safe for use in an MRI machine, i.e., safe without the feedback provided by regular monitoring of blood ethanol concentration which is difficult to perform in the MRI machine. A model of this type predicts physical measurements, but each parameter may not correspond to a physiological process. For instance, the parameter might be a time delay while the physiological process might be a complicated biochemical network that causes the time delay. However, the parameters in the model can be inferred from the available data, in this case OSIS signals, while the physiological process may be too complicated to be inferred.

Blood 'stealing' [37] is the idea that increased cerebral blood flow and volume in a region of tissue results in less flow and volume in surrounding tissue. A voltage source (pressure source) is used to describe the heart but if a voltage source drives a parallel connection of resistors and one resistor's value decreases leading to increased current through that resistor there is no effect on the current through the other resistors. Therefore, replacing the voltage source by a current source (flow source) or, most general among linear models, by a Thévenin equivalent circuit (a voltage source in series with a resistor), would probably make it easier to describe blood stealing.

Also related to blood 'stealing' is the control law for the Young's modulus of the vessel walls. In equations (17) and (18), Young's modulus is constrained to be between αE_0 and E_0, where E_0 is the resting value. Therefore, under no circumstances will the Young's modulus be greater than E_0, i.e., in no cases will the vessel further constrict. This could be changed to introduce a resting Young's modulus E_{rest} such that $\alpha E_0 < E_{\text{rest}} < E_0$ in which case vessels could constrict relative to the resting state which would cause blood 'stealing' and there is evidence for this modification [37].

A major issue is the overall topology of the microvascular network. An increasing number of network topologies are becoming available from TPLSM [10, 11]. A challenge is that they tend to fragment at depth, and so an estimation strategy that can determine a fully-connected network is a necessary and challenging part of using such networks in models of the type described in this paper.

We have used linear systems to describe the phenomenological control laws. However, delays may provide more parsimonious descriptions. Delay-differential equations are usually not finite dimensional. However, if the equations are solved by a forward-Euler approach and all delays are an integral multiple of the step size in the forward-Euler approach then it is still possible to solve the resulting equations in a straightforward manner.

Models constructed with these tools reproduce single-pixel OISI data from two different laboratories (figures 5 and 6) and reproduce the sublinear superposition seen with multiple stimuli (figure 8). While the number of parameters is large for single-pixel models (e.g., sections 3.1–3.4 and 4) the number of parameters is not large for describing the intra-operative clinical video [6] that motivates the model. The

unsolved challenge in applying the model to the clinical video is to determine the vascular topology from the video.

The methods described in this paper are really a toolbox for the construction of mathematical models rather than a single unique mathematical model. After having been validated on an initial set of experiments, such models can be used to predict the response to yet unperformed experiments. For example, predict the response of a mouse with polycythemia vera from the response of a normal mouse by changing just the blood dynamic viscosity parameter in equation (4) or predict the response of a mouse in an experiment done in a second laboratory with a second stimulus paradigm from the response of a mouse in the first laboratory with the first stimulus paradigm (by modification of equation (15)) thereby aiding in the comparison of results between laboratories. The range of prediction is likely limited to situations with fundamentally the same neurovascular physiology, e.g., the response of a subject undergoing spreading depression or an epileptic seizure is probably poorly predicted by a model validated with normal data. Finally, models of this type may be useful ways to summarize intra-operative clinical video [6].

While some of the variables and relationships between variables in the model described in this paper have physical meaning, e.g., vessel radius and Laplace's law, other variables do not, such as the homeostasis budget variable $e(t)$. In particular, $e(t)$ is inspired by the idea that a limiting reagent exists that can be replenished by blood flow. Although nutrients or oxygen might contribute to such a dynamic and the energy stored as ATP or NAD(P)H might follow this paradigm, this model is not intended to model the concentration of any particular substance (section 2.2.3). Furthermore, replenishment of a needed reagent can easily be replaced by removal of a waste product (section 2.2.3). An alternative process that would also have a feedback effect on vascular dynamics would be neurotransmitter recycling. Similar ideas to the ideas described in this paper might be applicable, e.g., the homeostasis budget variable $e(t)$ might be the mass of a particular neurotransmitter in the synaptic cleft. Neurotransmitter recycling involves multiple signaling mechanisms which might not necessarily be individually modeled, but instead simply lumped into an aggregate control law.

One unique and powerful feature of this model is that we were able to use a narrow range of parameters to both simulate neurovascular coupling responses to somatosensory stimulation and then use it to predict responses to other combinations of stimuli. Neurovascular-coupling based imaging is increasingly being used clinically as a potential diagnostic tool or surgical planning tool. The challenge in such applications is that there is high variability in the response of individual subjects. This model, which can use the response to a experimentally tractable stimulus to predict the response to another stimulus, could be a step in developing tools for such future applications.

Acknowledgments

NRC is grateful for financial support from Sandia National Laboratories in the form of a Sandia Laboratory Directed Research and Development Five-year Fellowship.

References

[1] Ma H, Zhao M and Schwartz T H 2013 Dynamic neurovascular coupling and uncoupling during ictal onset, propagation, and termination revealed by simultaneous in vivo optical imaging of neural activity and local blood volume *Cerebral Cortex* **23** 885–99

[2] Ma H, Geneslaw A, Zhao M, Suh M, Perry C and Schwartz T H 2009 The importance of latency in the focality of perfusion and oxygenation changes associated with triggered afterdischarges in human cortex *J. Cereb. Blood Flow Metabolism* **29** 1003–14

[3] Zhao M, Ma H, Suh M and Schwartz T H 2009 Spatiotemporal dynamics of perfusion and oximetry during ictal discharges in the rat neocortex *J. Neurosci.* **29** 2814–23

[4] Ma H, Zhao M, Suh M and Schwartz T H 2009 Hemodynamic surrogates for excitatory membrane potential change during interictal epileptiform events in rat neocortex *J. Neurophysiol.* **101** 2550–62

[5] Bahar S, Suh M, Zhao M and Schwartz T H 2006 Intrinsic optical signal imaging of neocortical seizures: the 'epileptic dip' *Neuroreport* **17** 499–503

[6] Suh M, Bahar S, Mehta A D and Schwartz T H 2006 Blood volume and hemoglobin oxygenation response following electrical stimulation of human cortex *NeuroImage* **31** 66–75

[7] Devor A *et al* 2012 Frontiers in optical imaging of cerebral blood flow and metabolism *J. Cerebral Blood Flow Metabolism* **1–18** 18

[8] Barrett M J P, Tawhai M H and Suresh V 2012 Arteries dominate volume changes during brief functional hyperemia: evidence from mathematical modelling *NeuroImage* **62** 482–92

[9] Reichold J, Stampanoni M, Keller A L, Buck A, Jenny P and Weber B 2009 Vascular graph model to simulate the cerebral blood flow in realistic vascular networks *J. Cerebral Blood Flow Metabolism* **29** 1429–43

[10] Nishimura N, Rosidi N L, Iadecola C and Schaffer C B 2010 Limitations of collateral flow after occlusion of a single cortical penetrating arteriole *J. Cerebral Blood Flow Metabolism* **30** 1914–27

[11] Shih A Y, Driscoll J D, Drew P J, Nishimura N, Schaffer C B and Kleinfeld D 2012 Two-photon microscopy as a tool to study blood flow and neurovascular coupling in the rodent brain *J. Cerebral Blood Flow Metabolism* **32** 1–33

[12] Buxton R B, Wong E C and Frank L R 1998 Dynamics of blood flow and oxygenation changes during brain activation: the Balloon model *Magn. Reson. Med.* **39** 855–64

[13] Mandeville J B, Marota J J A, Ayata C, Zaharchuk G, Moskowitz M A, Rosen B R and Weisskoff R M 1999 Evidence of a cerebrovascular postarteriole windkessel with delayed compliance *J. Cerebral Blood Flow Metabolism* **19** 679–89

[14] Zheng Y *et al* 2010 A dynamic model of neurovascular coupling: Implications for blood vessel dilation and constriction *NeuroImage* **52** 1135–47

[15] Huppert T J, Allen M S, Benav H, Jones P B and Boas D A 2007 A multicompartment vascular model for inferring baseline and functional changes in cerebral oxygen metabolism and arterial dilation *J. Cerebral Blood Flow Metabolism* **27** 1262–79

[16] Zhou J, Wilson D A, Ulatowski J A, Traystman R J and van Zijl P C M 2001 Two-compartment exchange model for perfusion quantification using aterial spin tagging *J. Cerebral Blood Flow Metabolism* **21** 440–55
[17] Boas D A, Jones S R, Devor A, Huppert T J and Dale A M 2008 A vascular anatomical network model of the spatio-temporal response to brain activiation *NeuroImage* **40** 1116–29
[18] Aubert A and Costalat R 2002 A model of the coupling between brain electrical activity, metabolism, and hemodynamics: Application to the interpretation of functional neuroimaging *NeuroImage* **52** 1162–81
[19] Grubb R L Jr, Raichle M E, Eichling J O and Ter-Pogossian M M 1974 The effects of changes in PaCO $_2$ cerebral blood volume, blood flow, and vascular mean transit time *Stroke* **5** 630–9
[20] Drzewiecki G, Field S, Moubarak I and Li J K-J 1997 Vessel growth and collapsible pressure-area relationship *Am. J. Physiol. Heart Circ. Physiol.* **273** 2030–43
[21] Zheng Y and Mayhew J 2009 A time-invariant visco-elastic windkessel model relating blood flow and blood volume *NeuroImage* **47** H1371–80
[22] Truskey G A, Yuan F and Katz D F 2009 *Transport Phenomena in Biological Systems* 2nd edn (Englewood Cliffs, NJ: Prentice-Hall)
[23] Washburn E W 1921 The dynamics of capillary flow *Phys. Rev.* **17** 273–83 2nd series
[24] Pries A R, Secomb T W, Gessner T, Sperandio M B, Gross J F and Gaehtgens P 1994 Resistance to blood flow in microvessels in vivo *Circ. Res.* **75** 904–15
[25] Pries A R and Secomb T W 2005 Microvascular blood viscosity in vivo and the endothelial surface layer *Am. J. Physiol. Heart Circ. Physiol.* **289** 2657–64
[26] Stryer L 1999 *Biochemistry* 4th edn (New York: Freeman)
[27] Paulson O B, Hasselbalch S G, Rostrup E, Knudsen G M and Pelligrino D 2010 Cerebral blood flow response to functional activation *J. Cerebral Blood Flow Metabolism* **30** 2–14
[28] Raichle M E and Mintun M A 2006 Brain work and brain imaging *Annu. Rev. Neurosci.* **29** 449–76
[29] Martin C, Martindale J, Berwick J and Mayhew J 2006 Investigating neural-hemodynamic coupling and the hemodynamic response function in the awake rat *NeuroImage* **32** 33–48
[30] Mathworks http://www.mathworks.com/
[31] Alle H, Roth A and Geiger J R P 2009 Energy-efficient action potentials in hippocampal mossy fibers *Science* **325** 1405–8
[32] Attwell D and Laughlin S B 2001 An energy budget for signaling in the grey matter of the brain *J. Cerebral Blood Flow Metabolism* **21** 1133–45
[33] Attwell D and Iadecola C 2002 The neural basis of functional brain imaging signals *Trends Neurosci.* **25** 621–5
[34] Lennie P 2003 The cost of cortical computation *Curr. Biol.* **13** 493–7
[35] Dunn A K, Devor A, Dale A M and Boas D A 2005 Spatial extent of oxygen metabolism and hemodynamic changes during functional activation of the rat somatosensory cortex *NeuroImage* **27** 279–90
[36] Plawecki M H, Han J-J, Doerschuk P C, Ramchandani V and O'Connor S J 2008 Physiologically-based pharmacokinetic (PBPK) models for ethanol *IEEE Trans. Biomed. Eng.* **55** 2691–700 PMID: 19126448
[37] Devor A, Ulbert I, Dunn A K, Narayanan S N, Jones S, Andermann M L, Boas D A and Dale A M 2005 Coupling of the cortical hemodynamic response to cortical and thalamic neuronal activity *Proc. Natl Acad. Sci. USA* **102** 3822–7
[38] Kasischke K A, Lambert E M, Panepento B, Sun A, Gelbard H A, Burgess R W, Foster T H and Nedergaard M 2011 Two-photon NADH imaging exposes boundaries of oxygen diffusion in cortical vascular supply regions *J. Cerebral Blood Flow Metabolism* **31** 68–81
[39] Vovenko E 1999 Distribution of oxygen tension on the surface of arterioles, capillaries and venules of brain cortex and in tissue in normoxia: an experimental study on rats *Pflugers Arch.* **437** 617–23